2.6 Physical Chemistry and Thermal Evolution of Ices at Ganymede

C. Ahrens, NASA Goddard Space Flight Center, Greenbelt, MD; caitlin.ahrens@nasa.gov

A. Solomonidou, Jet Propulsion Laboratory, California Institute of Technology, Pasadena, CA; & LEISA – Observatoire de Paris, CNRS, UPMC Univ., Paris 06, Univ. Paris-Diderot, Meudon, France; anezina.solomonidou@jpl.nasa.gov

K. Stephan, Institute of Planetary Research, German Aerospace Center (DLR), Berlin, Germany; katrin.stephan@dlr.de

K. Kalousova, Charles University, Faculty of Mathematics and Physics, Department of Geophysics, Prague, Czech Republic; klara.kalousova@mff.cuni.cz

N. Ligier, Institut d'Astrophysique Spatiale, Université Paris-Saclay, Orsay, France; nicolas.ligier@universite-paris-saclay.fr

T. McCord, Bear Fight Institute, Winthrop, WA; mccordtb@aol.com

C. Hibbitts, Applied Physics Laboratory, Johns Hopkins University, Laurel, MD; karl.hibbitts@jhuapl.edu

Abstract

Ganymede's surface is composed mostly of water ice and other icy materials in addition to minor non-ice components. The formation and evolution of Ganymede's landforms highly depend on the nature of the icy materials as they present various thermal and rheological behaviors. This chapter reviews the currently known thermodynamic parameters of the ice phases and hydrates reported on Ganymede, which seem to affect the evolution of the surface, using mainly results from the Voyager and Galileo missions.

Keywords: Ganymede; Ices; Ices, Mechanical Properties; Experimental techniques; Geological processes

1 Introduction

Icy bodies of the outer solar system, including satellites of the gas giants, harbor surface ices made of volatile molecules, clathrates, and complex molecules like hydrocarbons. Imaging of Ganymede's surface, as observed by the Voyager flyby and Galileo orbiter, reveals complex and mysterious geological structures composed of these materials and shaped by intricate physical processes. A major step toward understanding the nature of these geologic features on the Ganymedean surface and establishing their formational timescales and processes requires knowledge of the thermophysical and rheological properties of their composite material. Rheological information, like strength and flow, currently rests on laboratory-derived empirical relationships, which are essential for landform evolution and thermal modeling. Major science questions at Ganymede (and other icy satellites) and respective laboratory-

appropriate research offers a unique perspective for just how interdisciplinary thermophysical and rheological studies can be, as listed in Table 1.

Table 1: General overview of science questions at Ganymede in relation to respective experimental thermophysical properties.

Ganymede Science Questions	Laboratory Measurements/Properties
What is the composition and structure of the subsurface material?	Dielectric constant, viscoelasticity
What is the composition and structure of the surface material?	Strain rates, density, thermodynamic phase transitions
What are the power processes driving geological evolution?	Diffusivity, conductivity, viscosity, phase transitions
What are the radiative processes and surface evolution over short timescales?	Heat capacity, sublimation pressures, phase stability, latent heat

The Pioneer and Voyager flyby missions paved the way for NASA's Jovian system spacecraft Galileo (*Mura et al.* 2020). This spacecraft obtained results by an onboard magnetometer (MAG), solid-state imaging camera (SSI), the near-infrared mapping spectrometer (NIMS) operating in the range 0.7 – 5.2 μm, and the radio science experiment (*Carlson et al.* 1992). Further observations at infrared wavelengths of Ganymede were obtained by the flybys of the Cassini Visual and Infrared Mapping Spectrometer (VIMS) (*Brown et al.* 2004) and the New Horizons Linear Etalon Imaging Spectral Array (LEISA) (*Grundy et al.* 2007). From these instruments, the interior and surface processes have been estimated of Ganymede (see Chapter 2.1).

Ganymede's normalized moment of inertia (*Anderson et al.* 1996) and intrinsic magnetic field (*Kivelson et al.* 2002) suggest that it experienced enough heating for differentiation of a liquid iron core from the silicate mantle (see Chapter 2.1). *Vance et al.* (2018) suggests that the thickness of the hydrosphere probably exceeds 800 km, with the rock-ice interface at ~1.5 – 1.7 GPa. The internal ocean, sandwiched between the outer ice shell and deep high-pressure ice layer (e.g., *Vance et al.* 2014), is likely at a depth of ~160 km (ice I-III-liquid triple point), although its actual depth and thickness are not known (*Barr and Pappalardo* 2005). Ice shell thickness depends mainly on the rheological parameters of ice I (*Goldsby and Kohlstedt* 2001; *Barr and Pappalardo* 2005; see also Chapter 2.7).

The salinity of Ganymede's ocean is closely linked with the structure of the high-pressure ice layer and the stability of ice phases. Several studies have noted that briny fluids under pressure can have densities larger than those of high-pressure ices (*Vance and Brown* 2013; *Journaux et al.* 2013; *Vance et al.* 2014). While dense, salty fluids between HP ices are thermodynamically plausible to exist, the stability of such fluids requires further geodynamic modeling like that performed for purer oceans (*Kalousova et al.* 2018). In addition, the exchange processes between the silicate mantle and the ocean may also be affected by the presence of salts in the melt between the HP ice layer and the silicate crustal surface.

The surface of Ganymede (with a temperature range ~90 – 160 K) is a mix of water ice phases and darker non-ice materials (*Kieffer and Smythe* 1974; *Clark and McCord* 1980; *Mura et al.* 2020). Reflectance

spectra in the visible, infrared, and ultraviolet (namely through the NIMS aboard the Galileo spacecraft) indicate not only water ice, but may also be indicative of hydrated salts like on Europa (*McCord et al.* 2001) or other hydrated material (*Carlson et al.* 1999). Carbon dioxide (CO_2), sulfur (S = O bonds), oxygen (O_2) and ozone (O_3) molecules are also detected by visible and ultraviolet absorption features (*Nelson et al.* 1987; *Spencer et al.* 1995). While Hapke modeling is used as an estimation of the uppermost regolith physical properties (*Hapke* 1993), this is still dependent on the grain size, albedo effects, and optical properties of the regolith, which are poorly studied in the experimental setting.

In the thermophysical and rheological sense, ice can be considered as both a mineral and rock, as can the solar system's more volatile condensed species and hydrates. Past and present internal and surficial activity on the icy moons is driven by not only the frozen volatile components and respective phases, but also by internal and external energy sources (e.g., radiogenic, gravitational, tidal), and includes planetary surface-scale convection to localized relaxation of surface topography (*Durham et al.* 2010). Such landforms relax under gravitational forces controlled by the viscosity of the ice. Large impacts play several important roles for the rheological state of Ganymede's surface. Stirring of silicates from the ocean into the upper ice I layer by impacting may be important in controlling the ice viscosity. An impact may also trigger the merging of the ice I and HP ice layers and allow the heat pulse to occur, where the soluble impurities in the ocean would have otherwise made this spontaneous overturn impossible. Impacts can also puncture the lithosphere, allowing underlying warmer ice to flow onto the surface. This brings about an interesting relationship between exogenic and endogenic events of Ganymede (*Murchie et al.* 1990; *Spencer et al.* 1995).

Various ice phases and non-ice constituents have been estimated to fracture and flow, though understanding the material physics of the icy grains and rheological properties are difficult at relatively low temperatures (see Section 5) (*Parmentier* 1982; *Jankowski and Squyres* 1988; *Melosh and Janes* 1989). The purpose of this chapter is to present a current understanding of the temperature-dependent input thermophysical and rheological quantities and their implications for geomorphological processes on the Ganymedean surface, such as: density, viscosity, strain, thermal conductivity, and activation energies. In most experimental work, this information is relatively more complete in the pure ice forms, but currently poorly known are the complex mixtures that these ices may form.

1.1 Rheology in Cryovolcanism & Tectonism

As described in other chapters throughout this book, Ganymede possesses several tectonic and possibly cryovolcanic terrains in which understanding the thermodynamic and rheologic nature of the ices is vital to understanding the lithospheric properties for the resurfacing and tectonic strains involved.

The surface of Ganymede is rife with various levels of resurfacing from smooth to grooved terrains (see more in-depth reviews of these features in Chapter 2.2). On icy bodies in general, cryovolcanism is either the endmember of effusive eruptive deposits or explosive (*Smith et al.* 1982, 1986; *Squyres et al.* 1983; *Croft et al.* 1995). The eruption of liquid constituents through an ice-rich crust may seem difficult given the buoyancy difference of the melt compared to the solid (including the possible presence of contaminants, such as hydrates, that would vary its relative density), but can be accommodated due to the presence of volatiles that exsolve to decrease the density of the melt, or by the pressurization of a crustal melt or partial crystallization (*Fagents et al.* 2000).

The bright terrains present on Ganymede's surface may be indirect evidence for volcanic resurfacing, even with the lack of source vents and flow fronts. Resurfacing of smooth terrain has been noted to be analogous to lunar mare with shallow flooding from low-viscosity lavas and a general lack of major edifice structures (*Schenk et al.* 2001), and may share similar qualities, such as: (i) occupation at low-lying regions; (ii) embayed or partially buried craters and other rugged terrains; and (iii) large numbers of completely buried small craters. Smooth floors at the centers of impact basins and caldera-like structures are also unknown in their subsurface source (*Schenk and Moore* 1995; *Schenk et al.* 2001).

Extensional tectonism is responsible for the down-dropping blocks of dark terrain, extending both dark and bright terrains and resurfacing via grooved textures (e.g., flat-floored graben and flat-topped horst ridges like those at Uruk Sulcus) (*Collins et al.* 1998; *Schenk et al.* 2001). Images from Galileo have aided in the observation of brittle faulting (and some domino-style faulting) at the surface with additional imbrication of these faults on a scale of greatest local strain (*Golombek* 1982; *Pappalardo et al.* 1998; *Patel et al.* 1999), which also suggests that similar lithospheric properties are across Ganymede at the time of grooved terrain development (*Grimm and Squyres* 1985). Flexural modeling suggests local heat fluxes ~ 30 – 45 mW m^{-2} during deformation, consistent with extensional instability models, though this still depends on the ice phases and localized extensional tectonism (*Dombard and McKinnon* 2001; *Nimmo et al.* 2002; *Pappalardo et al.* 2003).

1.2 Landforms with Rheological Interest

It is with the variations of these Ganymedean morphologies that thermodynamical and rheological information must be required, which are discussed throughout this chapter. Here we discuss a brief overview of the different geologic structures that would have rheological aspects.

The fascinating bright furrowed terrain, called sulcus (pl. *sulci*), cross cutting the darker surroundings of Ganymede provides interesting insights into resurfacing and tectonic mechanisms, forming up to 66% of the Ganymedean surface (see Chapter 1.5 and 2.2 for more geologic information). Bright regions not necessarily associated with sulci are faculae, which also have implications of tectonism and resurfacing processes, typically labeled as palimpsests. The current implications of the emplacement of such brighter albedo formations include cryovolcanism or extensive heavily tectonized ice (*Shoemaker et al.* 1982; *Collins* 2000; *Schenk et al.* 2001). Such bright terrain burying older features indicates smooth terrains to be formed by flooding of shallow troughs with low-viscosity water ice lavas (*Schenk et al.* 2001; see Section 5.3). Sippar Sulcus exhibits topographic characteristics of icy volcanic resurfacing, consistent with low-viscous flooding of structural troughs to form the smooth terrains (*Schenk et al.* 2001). Such tectonism and deformations at sulci and faculae depend on the density and stresses of the ices (see Sections 5.2 and 5.4, respectively).

There are a variety of crater formations on the surface of Ganymede, including dark-floor, pedestal, palimpsest, penepalimpsest, multi-ring, and central peak (or dome) craters (*McKinnon and Melosh* 1980; *Schenk and McKinnon* 1991; *Schenk et al.* 2004; see Chapter 2.3). Numerical models (temperature-dependent and a power law stress-dependent viscosity for ice) of viscous relaxation of craters were purported to have relatively short relaxation times (t_e) for some carter depth to become reduced from an initial impactor state (*Thomas and Schubert* 1988). Newtonian rheologies appear to essentially dominate crater relaxation activity, though this applies when the effective temperature is several tens of degrees warmer than the surface (e.g., insulating regolith) or where the temperature gradients are considerably

small. This tends to be more so for crater diameters < 25 km (*Thomas and Schubert* 1988). However, non-Newtonian rheological laws can occur at larger craters and have relatively shorter relaxation times (for example, $t_e \sim 10^7$ years for crater diameters < 100 km). From *Dombard and McKinnon* (2006), relaxed craters in the Marius Regio suggest ancient heat flows with $\gtrsim 10$ mW m^2 (see Section 5.3). However, compositional constraints (e.g., silicious content) and dispersion hardening can extend these relaxation times. Modeling from *Thomas and Schubert* (1988) shows that a threshold crater diameter for the onset of non-Newtonian viscous behavior could not only estimate thermal gradients on a localized scale, but also localized stresses, although the variable-resolution from Galileo plus the current lack of experimental viscous ice research make this problem still unresolved.

Fossae (long, narrow depressions) and paterae (irregular, scalloped depressions) offer more interesting geomorphological structures relating to just how rheologically complex the surface of Ganymede is. Such scalloped textures could be considered caldera-like where these are sites of potential cryovolcanic vents (*Lucchitta* 1980; *Schenk and Moore* 1995). Fossae and their orientations also offer an interesting case for shear stresses (see Section 5.4) and brittleness of density-variable crustal material.

Dark terrain (*regiones*) comprises of nearly 1/3 of the Ganymedean surface with a greater fraction of non-ice and rocky material and showing a variety of modification by processes such as sublimation, mass wasting, ejecta blanketing, and tectonism (*Parmentier* 1982; *Prockter et al.* 2000). Based on impact crater counts, the dark terrain is considered ancient with an age > 4 Gy (see Chapter 2.3 for more details) (*Zahnle et al.* 2003). Also due to its low, heterogeneous albedo, this suggests thermally driven segregation of ice and non-ice constituents (*Spencer* 1987). For example, as observed in *Pappalardo et al.* (2004), Nicholson Regio imaged by Galileo is heavily tectonized with furrows (e.g., Anshar Sulcus, Byblus Sulcus), implying pre-existing weaknesses of the ice and non-ice densities.

2 Water Ice and other Volatile Phases

2.1 Water Ice Phases

The evolution of the outer solar system icy bodies has been significantly affected by the water ice, which can exist in three different solid configurations (amorphous, cubic, hexagonal) at low temperatures and pressures (*Jenniskens et al.* 1998). These different phases present large differences in their nature and behavior and have a considerable impact on the physical properties of ices on the solar system (*Mastrapa et al.* 2013). Nevertheless, the presence of amorphous and/or crystalline (cubic, hexagonal) water ice on a body depends on many factors, such as condensation temperature/rate, and its thermal history connected to the plethora of forms of irradiation, impact-heating and thermal variations (e.g., *Jenniskens et al.* 1998).

Amorphous ice – which seems to be the most common structure for H_2O in the Universe – has also been observed in much shallow layers (depths of μm) of the surfaces. There also exist different flavors of amorphous ices as well, including the high-density glassy water (HDG), which forms by vapor deposition at low temperatures (< 110 K) and irradiation, and could be a major phase present in many icy satellites (*Palumbo* 2005*; Giovambattista et al.* 2013).

During heating to a temperature between 110 and 150 K, amorphous ice transforms itself irreversibly to a cubic crystal structure and above 190 K, another irreversible transformation takes place, to the familiar hexagonal crystal structure (*Jenniskens et al.,* 1998). Water ice frozen from liquid water ice is always expected to crystallize with the hexagonal structure, and it maintains that structure, even when cooled to cryogenic temperatures (*Schmitt et al.,* 1998). Particularly, hexagonal ice should be abundant at the surfaces of solar system objects, freezing from standing water, cloud droplets, erupted water-rich melts, or impact melts (*Schmitt et al.,* 1998).

However, even though one would expect that energetic radiation would have destroyed the crystal structure and thus the remaining crystalline water ice on the Jovian, Saturnian, and Uranian icy satellites, it predominantly exists at the very shallow depths (mm) of their surfaces (*Grundy et al.* 1999; *Mastrapa et al.* 2013). The reason that crystalline water ice can exist under such large doses of radiation and thermal variations, is that at these locations, the temperature on the satellites reaches above 80 K (*Hansen and McCord* 2004).

The presence of water ice also affects the surface dynamics and morphology depending on its phase, especially in the bright terrains of Ganymede (*Allison and Clifford* 1987). Ganymede's total water abundance in the ice is ~30 – 50 wt.%, nearly up to ~90 wt.% in the shallow subsurface (e.g., *McCord et al.* 1998). There are also climatological dynamics at the polar regions being the result of transportation from the warmer equator to higher latitudes (*Clark* 1980; *Calvin et al.* 1995). The spectral signature (discussed in Chapter 2.5) can also tell us about grain sizes, ranging from a few hundred micrometers to a millimeter (*Pollack et al.* 1978; *Calvin et al.* 1995; *Hendrix et al.* 2013), where the equator and the trailing hemisphere of Ganymede have considerably larger grains of ice (*Stephan et al.* 2021). It should be noted that reflectance spectra and deconvolution techniques to determine ice abundances and phase species require some form of physical parameters obtained from experimental research, such as optical constants of different materials (*Grundy and Schmitt* 1998; *Dalton and Pitman* 2012), though these are temperature-dependent, and unfortunately lack experimental data at low temperatures (*Umurhan et al.* 2021).

The global pattern of ice phases present on Ganymede's surface indicates a balance between the crystallization and disruption processes. On Ganymede, mainly crystalline water ice is present at the equator where relatively high temperatures and lower radiation flux exist, whereas amorphous water ice can be predominantly found at Ganymede poles, which experience relatively low temperatures and higher radiation flux (*Hansen and McCord* 2004; *Ligier et al.* 2019). According to *Jenniskens et al.* (1998) as temperature varies between 105 K and 125 K, the crystallization of ice can vary by a factor of ~10^5. On Ganymede, the equatorial midday ice temperature varies by around 20 K, but from the equator to the poles, the temperature varies by approximately 10 K. This implies that a significant variation in crystallization rate as a function of temperature in the midlatitudes and polar regions is largely absent on Ganymede (*Hansen and McCord* 2004). Hence, it seems possible that other factors are controlling the disruption and crystallization functions on Ganymede, and these are not simply controlled by the thermal crystallization rates (*Hansen and McCord* 2004).

The triple point of H_2O is at 273.16 K and ~6.116 x 10^{-3} bar (*Wagner and Pruss* 2002). *Fray and Schmitt* (2009) collected several experimental measurements ranging from 130 – 273.15 K. Numerous experimental relations have been published to compute the vapor pressure of hexagonal water ice (Ih); however, the vapor pressure of cubic water ice (Ic) is ~10.5% higher than for Ih (*Washburn* 1924; *Yamamoto et al.* 1983; *Murphy and Koop* 2005; *Huebner et al.* 2006). Of note is the Ic phase is a metastable version of Ih (*Petrenko and Whitworth* 1999). All these works, and those included in the *Fray and Schmitt* (2009) summary have also shown that amorphous ice strongly depends on condensation

temperature and the rate of condensation. This dependence on condensation rate and temperature conditions basically applies to all forms of HP ices as well (*Mastrapa et al.* 2013). From observations from *Mastrapa et al.* (2013), amorphous ice will convert to crystalline structures within 10^4 years, wherefore amorphous ices are only consistently stable at colder (< 100 K) surfaces.

What is interesting for Ganymede, and icy bodies in general, are their hydrospheres, where there is variable amount of pressure (i.e., 0 – 1600 MPa). At this pressure range exist several icy polymorphs, including high-pressure (HP) ices (Ih, Ic, II, III, IV, V, VI, IX, XI, XII, XIII, XIV, and XV) (*Schmitt et al.* 1998; *Nakamura and Ohtani* 2011) as well as a suite of clathrate hydrates (see Section 3). Ice phases relevant to Ganymedean conditions are shown in Figure 1. While ice VI is expected to occur for any ocean composition (pure H_2O or aqueous solution of $MgSO_4$ or other relevant salts) and thermal profile, the presence of ice V and III is predicted only for dense salty oceans and cold interiors (*Vance et al.* 2018). Ice III can form at the base of the ocean underlain by ice V and VI, if the ocean is cold and its salinity is ~ 10 wt.% $MgSO_4$ (*Vance et al.* 2018). However, Ice III can be buoyant relative to modeled oceans, where dynamically short-lived ices may perhaps quicken the cooling of Ganymede and thicken the ice I crust, therefore accumulating underneath the ice I – ocean interface. From Figure 1, the gray area are conditions expected for large ocean worlds. This area encompasses ice phases I, III, V, VI and the water liquid phase. This area also includes conditions for the existence of ammonia hydrate dissociation (in the monohydrate phase), and other various clathrates at temperatures ~280 – 300 K.

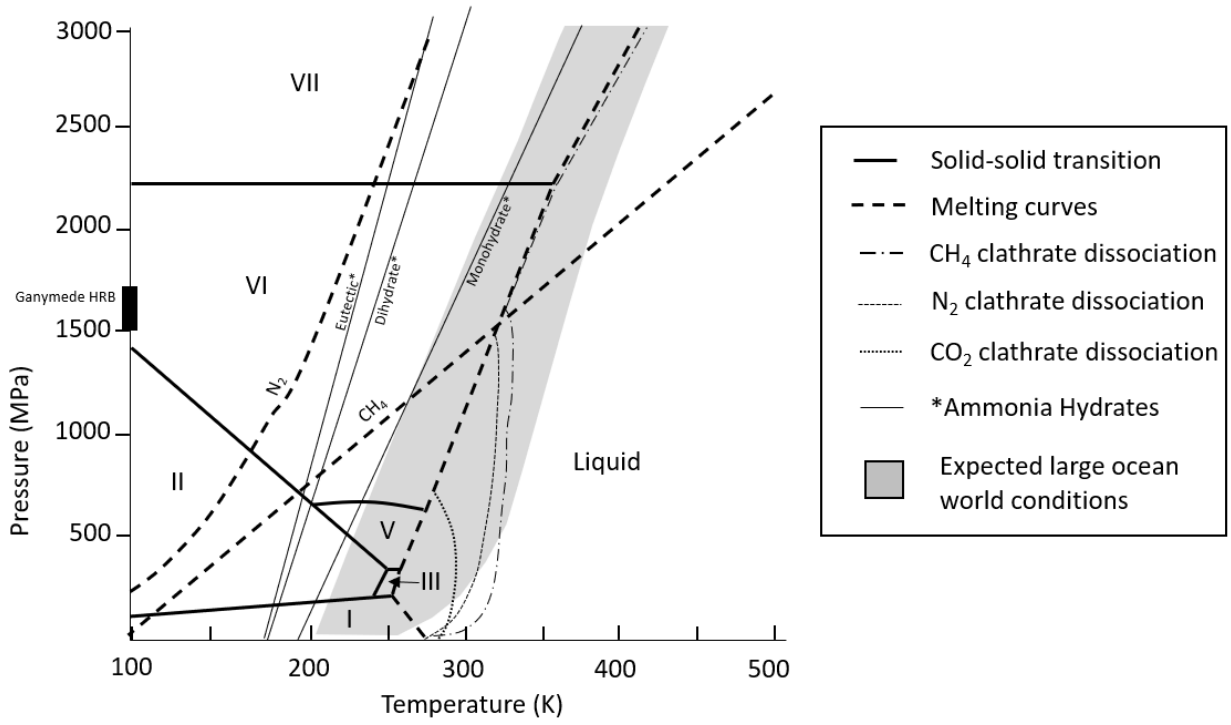

Figure 1: Temperature/pressure phase diagram of water ice polymorphs relevant to water-rich satellite interiors. Melting curves and solid-solid phase transitions are from *Journaux et al.* (2020). The shaded region corresponds to the estimated range of conditions expected in ocean worlds. Clathrate dissociation curves are from *Durham et al.* (1998). The hydrosphere-rock boundary (HRB) is adapted from *Journaux et al.* (2020).

2.2 Other Volatile Species

O_3 and O_2 have been found to be trapped in the surface ice within voids or bubbles, with O_2 predominantly existent in the equatorial region and O_3 dominating at the poles (*Nelson et al.* 1987; *Noll et al.* 1996; *Spencer et al.* 1995; *Johnson and Jesser* 1997; *Hendrix et al.* 1999) and have been interpreted to form by a combination of solar UV radiation and impacting magnetospheric plasma. The triple point of oxygen (O_2) is at 54.33 K and 1.49×10^{-3} bar (*Fray and Schmitt* 2009). Solid O_2 has three different crystalline phases (Table 2), the temperatures of the phase transitions are 23.78 K (α-β transition) and 43.77 K (β-γ transition) (*Mullins et al.* 1963). O_3 has disagreeable experimental research to find a triple point (*Fray and Schmitt* 2009). The data of *Hanson and Mauersberger* (1986) seem to be the better research collection, with the triple point of O_3 to be at 79.6 K and 5.6×10^{-6} bar.

Carbon dioxide (CO_2) presumably trapped in Ganymede's dark material is widely distributed. CO_2 has a triple point located at 216.58 K and 5.18 bar. Experimental and empirical data points have been collected from 69.69 – 216.56 K (Table 2), listed in *Fray and Schmitt* (2009). However, its origin on Ganymede is not clear. See Chapters 2.5 and 3.2 for a detailed discussion of the identification, distribution, and formation processes of these compounds. From observations by *Hibbitts et al.* (2003), CO_2 distributions appear to be controlled by geological processes, with combination effects from the Jovian (and Ganymedean) magnetospheres, finding that: (i) the deepest CO_2 bands are found in darker, non-icy material regions; (ii) CO_2 is not detected in the icy polar regions; (iii) Ganymede's upper crust is depleted of CO_2 (the exception is Mir crater); (iv) dark crater ejecta appear to be depleted in CO_2; (v) greater concentrations of CO_2 are correlated with areas of larger-grained ice; (vi) CO_2 detected by NIMS is mostly contained in the non-ice constituents; and (vii) CO_2 could exist in the large-grained ice near the equatorial and midlatitude regions, but currently this remains undetected by NIMS data due to the too large grain sizes.

Sulfuric acid hydrate and other sulfur compounds including SO_2 might be endogenic or could be the product of the bombardment of the icy surface by exogenous sulfur as well as sulfur molecules released by Io's very active volcanoes (*Calvin et al.* 1995; *Strazzulla* 2011; *Ligier et al.* 2019). Radiolysis can also play a major role in the forming of SO_2 and H_2SO_4 in either the ice or in water associated with Ganymede's hydrated non-ice material and the implantations of S-ions (*Hibbitts et al.* 2003; *Ligier et al.* 2019). The triple point of sulfur dioxide (SO_2) is 197.64 K and 0.0167 bar. The heat capacity of the solid has been measured (15.20 – 197.64 K) in *Giauque and Stephenson* (1938). Hydrogen sulfide (H_2S) triple point is at 187.57 K (0.229 bar). H_2S exists in three different crystalline forms (*Anderson et al.* 1977), where phase III transforms to phase II at 103.6 K and to phase I at 126.2 K.

Table 2: Temperature and pressure ranges for non-H_2O volatile species observed on Ganymede. Values from *Fray and Schmitt* (2009).

Species	Solid Phase	Temperature Range (K)	Pressure (bar)
O_2	α	20 – 23.78	$(1.49 \pm 0.03) \cdot 10^{-3}$
	β	23.78 – 43.77	
	γ	43.77 – 54.33	
O_3		< 79.6	$(5.6 \pm 0.6) \cdot 10^{-6}$

CO_2		40 – 194.7	5.185 ± 0.005
		194.7 – 216.58	
H_2S	I	126.2 – 187.57	0.229 ± 0.008
	II	103.6 – 126.2	
	III	< 103.6	
SO_2		15 – 197.63	0.0167 ± 0.0001

3 Hydrated Salts and Clathrate Constituents

Hydrates may have reached the surface on Ganymede at some point in the satellite's history. This is consistent with the interpretation of results from the Galileo magnetometer investigations, suggesting a conductive fluid layer (*McCord et al.* 2001; *Pappalardo et al.* 2004). This is also prevalent with the identification of observed surface disruptions, like those seen on Europa (*McCord et al.* 2001). Several studies have predicted such salts and hydrates to exist through exogenic and endogenic processes (*Kargel et al.* 2000; *Fanale et al.* 2001; *Strazzulla et al.* 2009). The thermodynamic modeling of these hydrates remains relatively unknown at higher pressures where the solubility and activity of many planetary-relevant gases is poorly constrained, particularly at lower temperatures (*Sloan and Koh* 2007; *Choukroun et al.* 2013).

Hydrated sulfates are anticipated to be a major component in rock-forming minerals in the interiors of the inner Galilean moons, probably from the result from the leaching of chondritic sulfates from their cores during differentiation (*Kargel et al.* 1991). Ganymede's magnesium-bearing sulfates and salts are similar to those observed on Europa (*McCord et al.* 1998). Similarly with sulfuric acid hydrates, the abundance on Ganymede is lower than on Europa.

Nakamura and Ohtani (2011) identified several phases in the $MgSO_4 – H_2O$ system up to 4 GPa at 298 K through laboratory experiments: Ices VI and VII, $MgSO_4 – 7H_2O$ (magnesium heptahydrate), and a liquid phase. These phase relations suggest that the liquid layer may be at a depth of ~800 km in the interior of Ganymede. The $MgSO_4$ content of the bulk icy mantle composition is ~15 – 20 wt.% (as modeled by *Kargel et al.* 1991), which is higher than the $MgSO_4$ eutectic (12 – 14 wt.% at 2 GPa), so its liquidus phase is likely ($MgSO_4 – 7H_2O$, referred to as *MS7*) hydrate at the base of the mantle, where ($MgSO_4 – 11H_2O$, referred to as *MS11*) is at shallower depths (*Nakamura and Ohtani* 2011). The eutectic between MS11 and ice Ih is at 269.25 K with 17.5 wt.% $MgSO_4$ (*Fortes et al.* 2010).

The low eutectic temperature indicates that the icy mantle may be molten, if not partially, and so the crystallization of the outer icy mantle is inevitable in the early stages of Ganymede's geologic evolution. A fractional crystallization of the icy mantle will produce a layered structure where the MS7 phase is at the bottom, an internal ocean close to the eutectic composition, covered by an icy crust (*Fortes et al.* 2010; *Nakamura and Ohtani* 2011). Based on *Zolotov and Shock* (2001), such layering could lead to Cl-salts at the top. However, the thickness of the icy crust and that of the bottom layer depend on the temperature profile of Ganymede, silicate grains and other possible hydrate mixtures involved, and heat flux from the inner silicate layer (where the internal ocean would be deeper) (*Hussmann et al.* 2006; *Bland et al.* 2009).

Clathrate hydrates are essentially skeleton-like cages of hydrogen-bonded H_2O molecules that trap neutral guest molecules (e.g., CH_4, N_2, CO_2, etc.). No bond occurs between the host and guest species, but a van

der Waals interaction stabilizes the structure. The cage structure depends on the pressure and temperature conditions and the nature of the guest species, where several species may occur at the same void space. CO_2 presents an interesting case as a flavor of clathrate in that a single CO_2 hydrate structure destabilizes into a filled, solid ice structure < 1 GPa (*Amos et al.* 2017; *Massani et al.* 2017). At conditions > 1 GPa, H_2O and CO_2 form a solid mixture (*Hirai et al.* 2010). However, at > 3 GPa, a change in the CO_2 speciation leads to greater solubility of C and the appearance of crystalline, hydrated carbonic acid (*Abramson et al.* 2018).

4 The "Darkening" Component

Before the arrival of Galileo, a great number of studies proposed that the non-ice (or frost-free) areas seem to be covered with a fine dust of carbonaceous chondritic material derived from ejecta from the outer irregular satellites, hence ancient meteoritic material (*Squyres* 1980; *Hartmann* 1980; *Schenk and McKinnon* 1991). Later, Galileo high-resolution images suggested that the dark material is composed of a relatively thin dark lag deposit of non-ice material overlying brighter icy material (*Patterson et al.* 2010). Roughly 34 – 35% of Ganymede's surface is ancient dark terrain that consists of a greater fraction of non-ice and rocky material (*Collins* 2000). *Murchie et al.* (1990) suggest that ammonia-rich fluids may also play a role in the dark deposits.

In a geophysical sense, dark terrain is suggested to be the product of a relatively thin lag deposit that punched through a thinner, more brittle lithosphere into a more mobile material (usually observed at the furrowed regions on Ganymede) and affected by a multitude of processes, such as sublimation, mass wasting and tectonism (*McKinnon and Melosh* 1980; *Prockter et al.* 2000).

These dark non-ice components are suggested to be endogenic at regions with increased fracturing or reactivation of pre-existing structures (*Shoemaker et al.* 1982; *Murchie et al.* 1986; *Prockter et al.* 2000). As mentioned earlier, the non-ice compounds could also originate from cryovolcanism, with the embayment of large diameter craters and smooth areas around furrows (*Croft and Strom* 1985; *Murchie et al.* 1989, 1990; *Lucchitta et al.* 1992). As water vapor is removed, a refractory material forms a sublimation lag and thus a darker surface. Over time, this low-refractory lag deposit may thicken for it to slough downslope. Based on the retention of small craters in dark terrains, the depth of the lag deposits is probably a few meters on slopes, but thicker in the topographic lows at furrowed regions (*Pappalardo et al.* 2004). Understanding that this may hinder low-albedo lag deposits or thicken from endogenic processes presents its own complexities as to how this dark material would play a role in the overall rheology.

5 Rheologic Considerations

5.1 Microstructure, Composition & Polymorphism

As we have reviewed, the surface of Ganymede presents a variety of ice polymorphs and non-ice constituents. The rheology of ice is mainly controlled by temperature, grain size, porosity, and stress with

the corresponding material parameters highly influenced by impurities (*Kubo et al.* 2009). Although the observed impurities exist only in small quantities, they could play a role in the deformation of Ganymede's crust, especially if they are transported deeper into the icy crust. Even more macroscopic mass transport of trapped species by tectonic processes as supposed on Europa (*Prockter and Pappalardo* 2000) could also carry impurities to Ganymede's ocean (see Chapter 2.7).

In the case of water ice (both crystalline and amorphous), it is accepted that the interatomic cohesive forces are generally strong in H_2O ice crystals owing to the strength and complexity of hydrogen bonds, and that the presence of dislocation or surface heterogeneities is the main cause of relative weaknesses (*Macmillan* 1972). The polymorphism of water ice, as described in this chapter, results in the formation of concentric ice shells in the outermost layers of a differentiated icy satellite consisting of a variety of phases (and thus densities) of ice (*Fortes and Choukroun* 2010). *Journaux et al.* (2020) have made considerable pressure-volume-temperature computations for ices III, V, and VI, to determine the values of the main thermodynamic properties (density, thermal expansivity, heat capacity, etc.) for 250 – 300 K temperatures using the computational SeaFreeze package that uses the Gibbs energy representation to derive all thermodynamic properties at proper P-T conditions. This approach constrains material parameters in a wide range of conditions and prevents their extrapolation outside the range of laboratory experiments which is not fully reliable.

The effect of chemistry also influences HP ices. For example, ice VI is the only HP polymorph with ice VII to have been investigated for salt incorporation. *Journaux et al.* (2017) found that even small amounts of salts incorporated can have a significant effect on lowering its density. The extent to which other planetary-relevant salts (e.g., $MgSO_4$, $MgCl_2$, Na_2SO_4, etc.) incorporated into HP ices remains unconstrained.

5.2 Density

The chemical differentiation and thermal evolution of the HP ice layers, and the silicate core (and any subsequent impurities), depend greatly on the relative densities of important phases and whether they tend to sink or float, and (if large enough) become isolated from the residual liquids. The low viscosity and large density differentials of phases in salt-water brines should result in effective fractional crystallization of brine flows plus water ice would float to the top, and the salt hydrates would sink. Other works for density estimates can be found for water ice polymorphs (*Bridgman* 1912; *Journaux et al.* 2020); ammonia-water systems (*Croft et al.* 1988); and saline solutions (*Kargel et al.* 1991; *Hogenboom et al.* 1995).

For water ice polymorphs, *Jenniskens et al.* (1998) documented comparative density values between crystalline and amorphous water ice phases. For hexagonal ice (Ih), the density is ~0.93 g cm^{-3}, comparably the same as cubic ice (Ic), both at temperatures 120 – 150 K. Main phases of amorphous ice are based on density: I_ah (high-density amorphous) = 1.1 g/cm^3 (*Narten et al.* 1976) and low-density amorphous (I_al) = 0.94 g/cm^3 (*Jenniskens and Blake* 1994). However, these experiments did not take porosity into account. At 90 K, the bulk density of water ice (from vapor deposition) is 0.82 g/cm^3, while at 35 K the density is 0.74 g/cm^3 (Ih) or 0.68 g/cm^3 (I_al with higher deposition rates) (*Narten et al.* 1976; *Brown et al.* 1996; *Berland et al.* 1996). At Ganymede, the upper HP ice layers (ice III) are modeled to be ~1.166 g/cm^3 while the lower, deeper ice VI is ~1.396 g/cm^3 (*Journaux et al.* 2020).

In the pure H_2O setting, all HP phases are denser than liquid water. However, the inclusion of salts (e.g., $MgSO_4$) would significantly alter the liquid density which may lead to density inversions and formation of layers (*Vance et al.* 2014, 2018). For non-ice materials, *Kargel* (1998) has summarized several densities for salts and saline solutions pertinent for briny volcanism and large ocean worlds. In Figure 2, there are several potential hydrate and salt solutions that can be present at Ganymedean surface conditions.

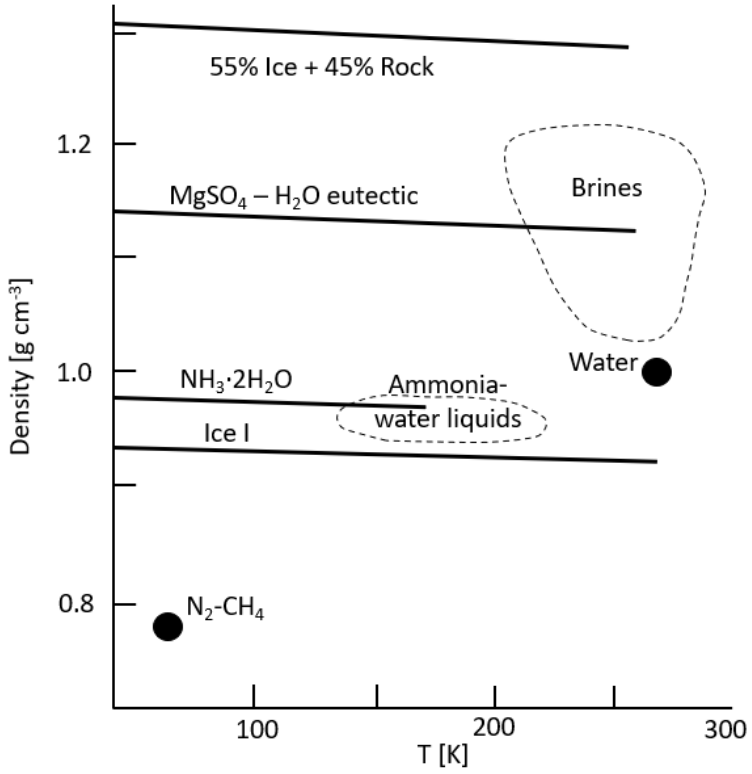

Figure 2: Ice I and cryofluid material densities across temperatures relevant to Ganymede. Also included is the $MgSO_4$-H_2O eutectic. Adapted from *Kargel* (1998).

5.3 Deformation & Viscosity

From a thermodynamic perspective, if the ice flows readily internally, the satellite is cooling. Though if the ice resists, the satellite will overheat, or essentially melt internally and increase its differentiation (*Durham* 2010). Such warmer ice flowing in the subsurface against a relatively colder crust may be sufficient to overcome the strength of the crust, which will cause crustal failure. Ice flow owes its origins to glaciologic laboratory studies to create the *Glen law* for the creep behavior of polycrystalline ices, including the applications of strain rate and shear stresses (discussed in Section 5.4).

Creep is defined as a general term in which volume-conserving deformation mechanisms involve the motion of grain-boundary or crystal-lattice defects (*Poirier* 1985). On geologically long timescales (millions of years), ice deforms via viscous deformation. The deformation mechanism depends on the

local stress and temperature conditions as well as on the ice grain size. Based on laboratory experiments, three distinct mechanisms were described (e.g., *Goldsby and Kohlstedt* 2001; *Durham et al.* 2001; *Umurhan et al.* 2021): grain boundary sliding, basal slip, and dislocation creep. All these mechanisms are nonlinear, i.e., strain-rate $\dot{\varepsilon}$ and stress σ are not linearly related:

$$\dot{\varepsilon} = \frac{A}{d^p}\sigma^n exp\left(\frac{-Q}{RT}\right) \quad (1)$$

Here A is a pre-exponential constant, d is the grain size with p its exponent, n is the stress exponent, Q is activation energy, R the universal gas constant, and T the temperature. Viscosity, i.e., the ratio between stress and strain-rate, is thus stress-dependent.

For very high stresses (>1MPa) and large grains, deformation is accommodated by the movement of dislocations in the crystal lattice. Dislocation creep (disl) is highly nonlinear and is characterized by the stress exponent of $n=4$. However, viscosity does not depend on the grain size. Enhanced deformation is observed if temperatures are within 15 K from the melting curve. For lower stresses (between ~0.01 and 1 MPa), grains deform along the crystal planes by basal slip (bs). In crystals, whose planes are not well oriented for basal slip, another process occurs to accommodate deformation, the grain boundary sliding (gbs). These two mechanisms are not independent but act together and are combined as follows (*Goldsby and Kohlstedt* 2001):

$$\dot{\varepsilon}_{gss} = \left(\frac{1}{\dot{\varepsilon}_{gbs}} + \frac{1}{\dot{\varepsilon}_{bs}}\right)^{-1} \quad (2)$$

into so-called grain-size sensitive creep (gss). However, only grain boundary sliding viscosity depends on the grain size ($p=1.4$) while basal slip viscosity is grain size independent ($p=0$). Both mechanisms have stress exponent close to 2 ($n=1.8$ for gbs and 2.4 for bs). Finally, for even lower stresses, relatively high temperatures (≳150 K) and small grain sizes (< 1 mm), ice deforms by the diffusion of vacancies through the crystal lattice. Diffusion creep (diff) is a linear mechanism ($n=1$) so its viscosity does not depend on stress. It depends on the square of the grain size ($p=2$).

Altogether, the four mechanisms combine as:

$$\dot{\varepsilon} = \dot{\varepsilon}_{diff} + \dot{\varepsilon}_{gss} + \dot{\varepsilon}_{disl} = \dot{\varepsilon}_{diff} + \left(\frac{1}{\dot{\varepsilon}_{gbs}} + \frac{1}{\dot{\varepsilon}_{bs}}\right)^{-1} + \dot{\varepsilon}_{disl} \quad (3)$$

(*Goldsby and Kohlstedt* 2001). This flow law fits the laboratory data. For a more detailed review and the values of all parameters, see *Durham and Stern* (2001) or *Barr and Showman* (2009). Depending on the grain size which can range between <1 mm and a few cm, viscosity at the melting temperature (boundary with the ocean) is between 10^{13} and 10^{16} Pa s. At the surface, the experimentally-derived flow law

predicts too large viscosity values (>10^{20} Pa s), indicating that other mechanism (elasticity or brittle failure) accommodates the stresses. In numerical models, an Arrhenius-type viscosity law is often used, that takes into account the most important effect of temperature but neglects the stress dependence (e.g. *Han and Showman* 2008).

The viscosity of high-pressure ices has been measured in the experimental setting (*Sotin et al.* 1985; *Durham et al.* 1996). The deformation of ice VI has been measured at large values of shear stress (10^8 Pa; *Sotin et al.* 1985) and found to have deformation rates of ~10^{-2} s^{-1} and a viscosity of 10^{10} Pa s. Extrapolation of these results to typical convective shear stresses (10^3 – 10^5 Pa) gives viscosities on the order of 10^{12} – 10^{14} Pa s, similar to the ice I viscosities at the melting point, as observed in field measurements by *Hudleston* (2015). *Durham et al.* (1996) measured the viscosity of ice VI at comparably smaller pressures and found stronger stress dependence (e.g., larger values of the stress exponent *n*) and larger melting-point viscosity values. The discrepancy between viscosities predicted by these two studies may be due to different experimental conditions. Alternatively, a change in deformation mechanisms observed for ice Ih (e.g., *Goldsby and Kohlstedt* 2001), may be occurring in the HP phases as suggested by *Kalousova et al.* (2018), although no laboratory experiments were so far performed to confirm this hypothesis. Both studies (*Sotin et al.* 1985; *Durham et al.* 1996) suggest that viscosity is nearly constant along the melting curve, justifying the use of Arrhenius Law in numerical simulations (*Kalousova et al.* 2018). Due to the extrapolation from the high stress laboratory experiments to smaller-stress conditions and large uncertainty in grain size, numerical simulations usually consider a wide range of melting-point viscosity values between 10^{13} – 10^{17} Pa s (*Choblet et al.* 2017; *Kalousova et al.* 2018; *Kalousova and Sotin* 2018). Ice V viscosity, compared to ice VI, can be determined at the transition point between the two phases. *Sotin and Poirier* (1987) found that ice V is harder to deform than ice VI with their viscosity ratio being close to two orders of magnitude at the experimental conditions, while *Durham et al.* (1996) found that ice VI and ice V deform in a similar manner. Finally, ice III is the weakest in deformation (*Durham et al.* 1997).

Ice viscosity may get as low as 10^{10} Pa s if other cryogenic liquids are present, such as methane or NH_3 hydrates, suggesting that solid-state pure water ice is less likely to explain observed flow features or overall smoothing (*Stevenson and Lunine* 1986; *Schenk and Moore* 1995). Ammonia-water systems may also be important in investigating viscous flows (*Lunine and Stevenson* 1982). *Kargel et al.* (1991) observed that the behavior of ammonia-water eutectic and peritectic liquids resemble closely to basaltic behavior. Brines also have water-like viscosities (*Kargel et al.* 1991; *Hogenboom et al.* 1995).

Several viscosity-related processes may have acted on Ganymede's surface, such as mass wasting, erosion, and impact crater relaxation (*Parmentier* 1982; *Dombard and McKinnon* 2006). For example, Gilgamesh floor deposits with thickness of ~150 m and ~10 km across (as upper limits) have an estimated viscosity of ~10^6 Pa s, similar to ridges at Miranda and domes on Enceladus (Figure 3). Smooth surface materials have viscosities of ~10^6 Pa s with yield strengths of 0.2 kPa (*Schenk and Moore* 1995). These are in range of materials to behave (and deform) plastically with these viscosities and yield strengths. Alternatively, a partially crystalline melt could also be extruded, though achieving significant topography (> 150 m) may not be possible due to its extreme low viscosity. Assuming that the caldera-like floor materials (cryolava) were continuous extrusions and had a thickness of ~300 m, *Schenk and Moore* (1995) estimated their viscosities to be 10^{10} Pa s with yield strengths of ~10 kPa. Comparably, domes on Europa have 10^6 – 10^8 Pa s viscosity estimates, with yield strengths of ~1 – 10 kPa (*Schenk and Moore* 1995), somewhat weaker than on Ganymede.

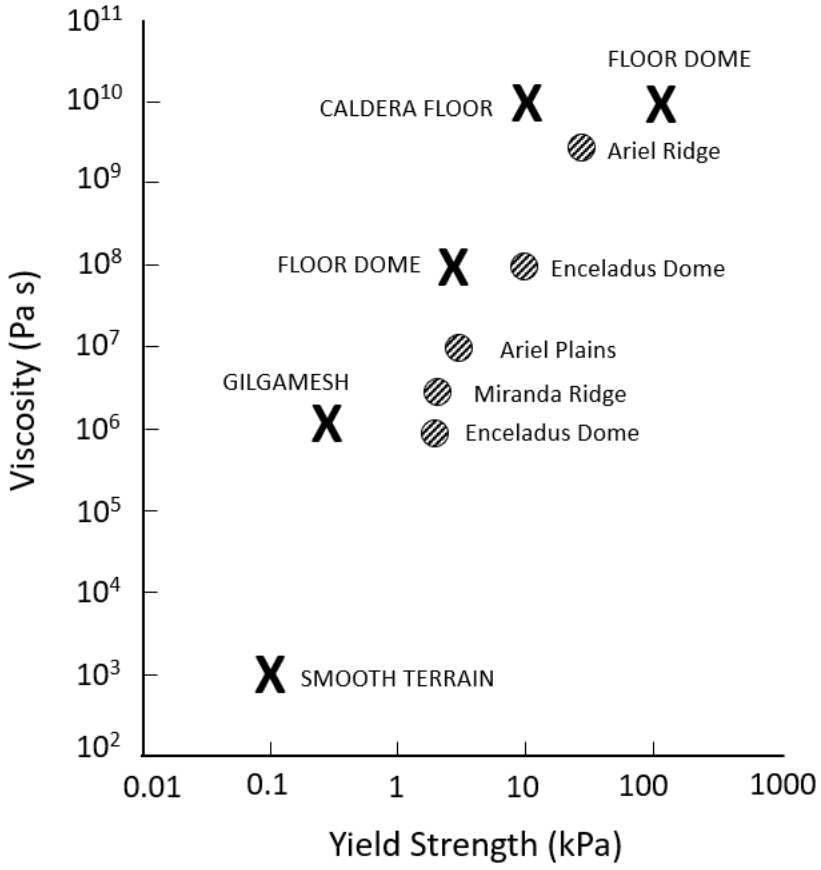

Figure 3: Rheologic strength versus viscosity of Ganymedean surface units compared to features from Enceladus, Miranda and Ariel. Adapted from *Schenk and Moore* (1995).

5.4 Stress & Strain Behavior

Ductile flows result in the deformation (strain ε) at a strain rate ($\dot{\varepsilon}$) that depends on several factors, including temperature, pressure, and effective grain size of the ice. Ice has a strength at failure nearly independent of temperature, but confining on pressure, namely in the range $0 < P < 50$ MPa. Brittle behavior is regulated by frictional properties, although these are less scale-dependent and therefore rudimentary to extrapolate from laboratory data, at least for the uppermost layers of an icy moon (*Schulson* 1979; *Petrenko and Whitworth* 1999; *Durham and Stern* 2001). Frictional strength strongly depends on pressure, not so much on temperature, and so increases with depth. Ductile strength, however, depends on temperature, thus decreasing with depth.

Strain is a relative measure of how much an ice substance of a certain size stretches or deforms. Stress is a measure of the internal forces and is defined in terms of a force per unit area (i.e., pressure). Generally, a block of polycrystalline ice subjected to some amount of applied stress (e.g., compressive, tensile, or shear) will respond with either ductile (or plastic) flow or will experience brittle fracture failure when the applied stress exceeds the material's yield stress (or elastic motions if the applied stress is less than the yield stress).

To describe elasto-viscoplastic rheology (see *Dombard and McKinnon* 2006 and references therein), the total strain is a linear summation of the elastic, viscous, and plastic strains (a Maxwell viscoelastic solid extended to include plasticity). Such an extended Maxwell solid captures the relative behavior on different geologic timescales, thus it behaves as a solid (elastic) material on shorter timescales, as a viscous (fluid) material on longer timescales and exhibits brittle (plastic) failure should the yield strength be exceeded (*Durham and McKinnon* 2006). Linear, isotropic elasticity can be characterized by two main parameters: *Young's modulus* (E) and *Poisson's ratio* (ν). While these parameters are inherently compressible, as *E* approaches infinity, the elastic response trends to incompressibility. For relaxation modeling on Ganymede, some use the values by *Dombard and McKinnon* (2006) of water ice *E* = 9.33 GPa and ν = 0.325.

Cryolava and viscoplastic rheologies flow with a viscosity η if bulk strength τ_0 is exceeded. Yield strength is estimated from the shape of the flow, assuming it has ceased movement (*Blake* 1990; *Schenk and Moore* 1995) where

$$\tau_0 = \frac{\rho h^2 g}{3r} \qquad (4)$$

and *h* and *r* are the height and radius of the flow, respectively. Flow viscosity estimates would need a time duration of the flow (*Huppert et al.* 1982), though this can only be deduced theoretically on icy bodies, especially with a lack of laboratory research at relatively low temperatures.

The bulk elastic properties of an ice are the ratio of the pressure change to the fractional volume compression. The ratio of the stress to the strain, regarding compressional forces, defines the Young's modulus. Both variables give us insight to the planar forces that can be supported at icy satellites and the pressure-temperature conditions that an ice sample can endure. Table 3 shows Ganymede-relevant ices and their respective Young's or bulk moduli.

Table 3: List of ice compounds and relevant Young's (*E*) or bulk moduli (*B*). Table adapted from *Umurhan et al.* (2021) and references therein. Ice III and VI modeled from *Vance et al.* (2018).

Ice Species	Modulus Type	Temperature (K)	Modulus (GPa)
Ice Ih	E	< 273	0.009 – 0.0112
	E	90	0.1 – 0.5
	E	100	0.2 – 0.9
CO_2	E	80	13.12
CH_4 clathrate SI	E	< 273	8.4
	B	< 273	8.76
CH_4 clathrate SII	E	< 273	8.2
	B	< 273	8.48
NH_3-H_2O	E	90	0.85
	E	100	0.1
Ice III	B	250	9.761
Ice VI	B	300	20.27

The inverse dependence of viscosity on stress (e.g., high stress corresponds with low viscosity and vice versa) results in significantly enhanced flow in regions of high stress (*Dombard and McKinnon* 2006). In impact craters, these high stress regions occur beneath the crater floor center, then as the crater bowl relief is reduced, the stress radiates outward to under the crater rim. Such stresses indicate movement of material down and away from positive topography and under negative topography, for example the rim and cavity of an impact crater, respectively (*Dombard and McKinnon* 2006). The surface tensile and basal layer compressive stresses are at the crater center, and the surface compressive and basal layer tensile stresses are along the periphery.

5.5 Thermal Conductivity

Thermal conductivity (λ) is defined as the bulk property for condensed matter and a main element for the magnitude (and resultant type) of geologic activity on planets and satellites. Thermal conductivity models tend to rely on pure ice Ih parameters, but this variable relies on the composition, porosity, crystallinity, and temperature/pressure conditions, all of which are highly variable on icy satellites (*Ross and Kargel* 1998; *Umurhan et al.* 2021). The thermal conductivity is a prime element in determining the physical processes related to cryovolcanism, mantle convection, viscous relaxation, and differentiation – each playing a role at the Ganymedean surface in some form or other.

Ice Ih to a degree is considered disordered in its crystallinity in that it exhibits nonzero entropy as temperature decreases, therefore not necessarily conforming to the third law of thermodynamics. For an overview of the disorder of crystalline materials and their respective thermal conductivities, see *Ross et al.* (1981). Both ice Ih and HP ices show a variation in thermal conductivity which is nearly proportional to the inverse of temperature (*Ross and Kargel* 1998; *Andersson and Inaba* 2005). Over the relevant temperatures, the ice Ih thermal conductivity (Figure 4) ranges from ~ 2 W m^{-1} K^{-1} at the ocean interface to ~6 W m^{-1} K^{-1} at the icy moons' surfaces. The lower thermal conductivities of ices II and III suggests the possibility of layers within an icy mantle that could exceed their melting point, producing cryovolcanic fluids (*Fortes and Choukroun* 2010).

The existence of a maximum thermal conductivity at low temperatures is characteristic of crystalline substances (*Klinger* 1973). The other extreme for thermal conductivity arises for amorphous materials where thermal conductivity is relatively small (< 1 W m^{-1} K^{-1}) and exhibits a monotonic and very minuscule increase with T. Figure 4 illustrates the extreme forms of thermal conductivity over temperature, comparing crystalline water ice phases and amorphous ices. However, there is disagreement over the thermal conductivity of amorphous ice as determined from laboratory work, which has also been suggested, for instance, to be 10^{-5} W m^{-1} K^{-1} by *Kouchi et al.* (1992).

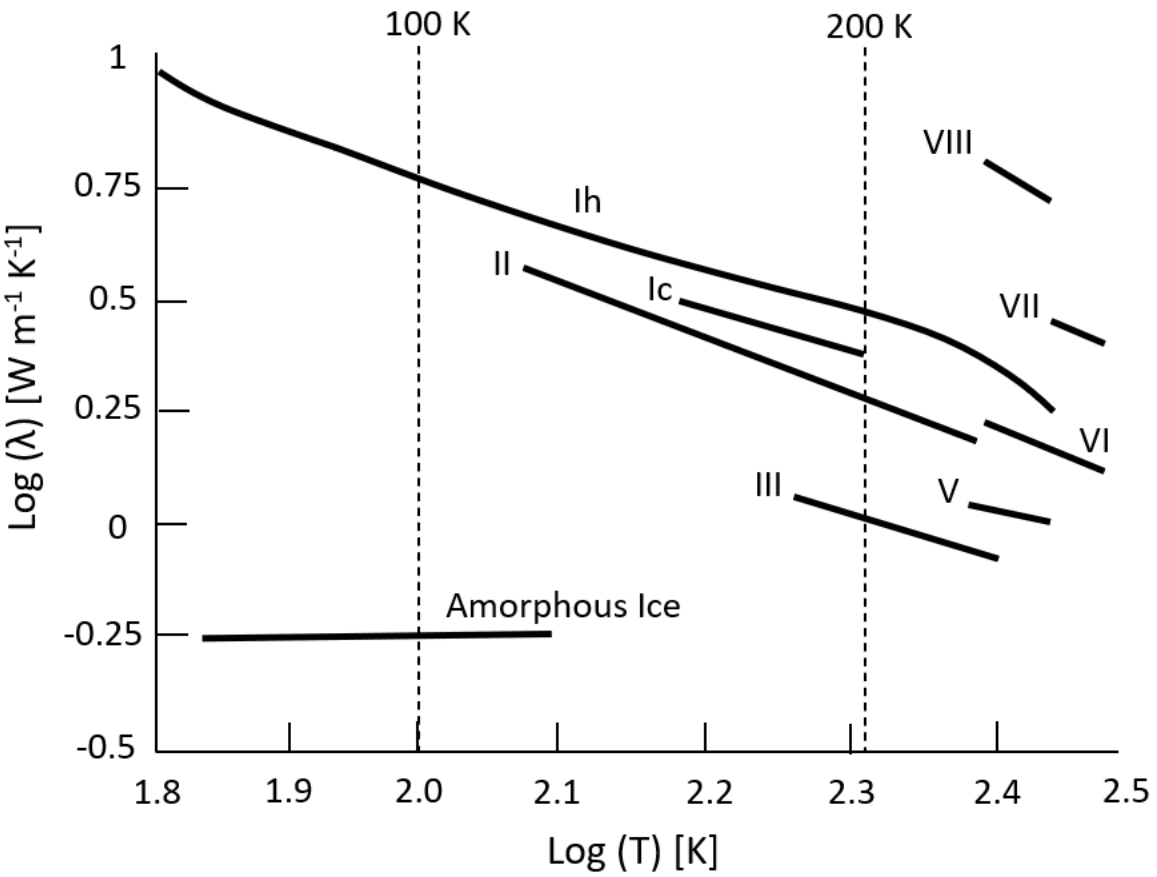

Figure 4: Thermal conductivities of water ice polymorphs in Ganymede-relevant temperatures. Note the lower thermal conductivity of amorphous ice compared to the crystalline water phases. Adapted from *Ross and Kargel* (1998).

5.6 Activation Energies

Activation energy is defined as the energy which an ice must possess to go through a physical or chemical reaction. Models relating the activation energy of the ice flow law and the critical Rayleigh number were derived by *Solomatov* (1995) and have been used to determine the conditions required to start convection in an ice shell (*Pappalardo et al.* 1998; *McKinnon* 1999). The activation energy of the ice sample indicates the material's Arrhenius temperature dependence reflecting the interior grain susceptibility to deformation (*Umurhan et al.* 2021). That is, the activation energy is usually the sum of a free energy activation energy plus an activation energy volume which considers the pressure dependencies.

Activation energies pertinent to ductility of ice has been reported in *Leonteva et al.* (1970) and *Yamashita et al.* (2010). Nucleation activation energy of amorphous (solid) water is 158 kJ/mol while the activation energy of crystal growth is ~47 kJ/mol (*Safarik and Millins* 2004). *Sugisaki et al.* (1969) observed that the activation energies of cubic ice (at 160 – 200 K) is ~21.3 kJ/mol where the hexagonal phase at those same temperatures have an activation energy of ~44.7 kJ/mol.

Sublimation energy is the heat required to change an icy constituent from solid phase to the gas phase. From current experimental results, CO_2 and NH_3 have higher sublimation energies than CH_4 and CO by a factor of ≥ 2 (see *Luna et al.* 2014). CO_2 at 80 – 90 K, the sublimation energy is 22.37 kJ/mol, then increases to 29.3 kJ/mol at 91.5 – 92.5 K (*Luna et al.* 2014).

These energies, though often experimentally with pure ices, are mostly inferred from theoretical predictions based on observed timescales of stress relaxation (*Leonteva et al.* 1970). This thermally dependent mechanism for activation (and sublimation) energy has only been explored for pure ice samples in an experimental setting, so more work certainly needs to be accomplished regarding mixtures and hydrate-type components relevant for Ganymede.

5.7 Rheologic Properties of Clathrates

Clathrates are very peculiar thermodynamically compared to water ice. The H_2O skeleton strongly resembles the ice Ih structure on an atomical level from Raman and infrared studies (*Nakano et al.* 1998; *Dartois and Deboffle* 2008; *Dartois and Schmitt* 2009). However, the presence of guest gases dramatically influences the molecular interactions and subsequently their thermophysical properties. Thermodynamically, some clathrate hydrates are similar to that of water ice. For example, the thermal expansion, heat capacity and elasticity of the CS-I and CS-II (clathrate structures) are very similar to ice Ih (*Choukroun et al.* 2013). While clathrates are usually more stable than water ices at MPa – GPa pressures, the stability is dependent on the abundance of the guest species in the environment (*Sohl et al.* 2010; *Choukroun et al.* 2013). Clathrate hydrates with volatiles like N_2, CH_4, or CO_2 are generally less dense than HP ices, but can achieve buoyancy or sink in aqueous solutions (*Journaux et al.* 2020).

Thermal conductivity has been the subject of numerous studies (e.g., *Ross et al.* 1981; *Cook and Leaist* 1983; *Tse and White* 1988), some of which noted a glass-like behavior that is temperature-dependent. At temperatures below 100 K, the conductivity increases, as expected from crystalline materials (*Tse and White* 1988; *English and Tse* 2010). On average, the thermal conductivity of clathrate hydrates is 0.4 – 0.7 W m^{-1} K^{-1} at pressures lower than 100 MPa and temperatures 100 – 270 K (*Choukroun et al.* 2013). The methane DO-clathrate (a 1.3-dioxolane clathrate type) has been measured to have a higher thermal conductivity than solid CH_4 uniformly with temperature by a factor of > 10 (*Ahmad and Phillips* 1987). Such a large difference could indicate how porosity and the cage-like structure of a clathrate can affect thermal conductivity. *Lorenz and Shandera* (2001) recorded an NH_3 ice sample (with 16% molar ratio of NH_3: H2O) being ~48% lower in thermal conductivity than pure water ice. *Sumarokov et al.* (2003) noted that CO_2 reaches relatively higher thermal conductivities at low temperatures up to ~700 W m^{-1} K^{-1}.

Despite the elastic properties being somewhat similar, the flow properties of clathrates have been subject to recent studies (e.g., *Stern et al.* 1996; *Durham et al.* 2005). Mechanical experiments conducted under high differential stress with a sustained gas pressure within the samples have reported that: (i) the initial results were likely due to significant dissociation (~30%); (ii) gas hydrates exhibit a much greater strength than water ice in that the strain rate requires applying a stress 10 – 30 times greater for clathrates than for water ice (*Choukroun et al.* 2013). Note that density values in Table 4 have been omitted due to their extreme variability and preliminary measurements dependent on the temperature, pressure, and guest gas molecule (*Sloan and Koh* 2007; *Choukroun et al.* 2013).

664 The rheological properties of clathrate hydrates have serious implications for the structures and processes
665 of ices and icy worlds (see Table 4). With variations in density, structure, occupancy, and guest species,
666 these parameters can create such complex mechanisms, though unfortunately still poorly known
667 experimentally. Combined with larger viscosity, the clathrate hydrate may form mechanically stiffer
668 thermally-insulating layers, which are particularly interesting for ice-ocean interfaces of icy bodies
669 (*Kamata et al.* 2019).

670

671 **Table 4:** Physical property comparison between water ice Ih phase and clathrate hydrates based on cage
672 structures (CS) – I and II. Values from *Choukroun et al.* (2013).

Physical Property	Ice Ih	Clathrate CS I	Clathrate CS II
Dielectric constant (at 273 K)	94	58	58
Young's modulus (at 268 K) [GPa]	8 – 9.5	8.5	8.5
Poisson's ratio	0.331	0.31403	0.31119
Thermal Expansion (at 200 K) [10^{-6} K^{-1}]	56	77	52
Thermal Conductivity (at 263 K) [W m^{-1} K^{-1}]	2.18	0.51	0.50

673

674 **6 Summary**

675

676 As we have observed through this chapter, the thermodynamic and rheologic properties of ice phases and
677 hydrates remain mostly theoretical and we note that more experimental measurements are needed. Our
678 knowledge of Ganymede's surface composition has greatly improved our modeling and understanding of
679 spectral behaviors, but it is the complexity and diversity of Ganymede's surface that we must peer
680 through to understand the thermal properties of these variable ice phases. Their physical parameters, such
681 as grain size and density, are key to understanding the endogenous and exogeneous processes, especially
682 in modeling the HP ice layer and geologic formations. We hope this chapter is used as a compendium for
683 thermodynamic parameters of ice phases and hydrates relevant to Ganymede.

684

685 **Acknowledgements**

686 C. Ahrens' research was supported by an appointment to the NASA Postdoctoral Program at the NASA
687 Goddard Space Flight Center, administered by Universities Space Research Association under contract
688 with NASA.

689 K. Kalousova was supported by the Czech Science Foundation through project No. 19-10809S and by
690 Charles University Research Program No. UNCE/SCI/023.

691

8 References

Abramson, E., Bollengier, O., Brown, J., Journaux, B., Kaminsky, W., Pakhomova, A. (2018). Carbonic acid monohydrate. American Mineralogist: Journal of Earth and Planetary Materials, 103(9), 1468-1472.

Ahmad, N., and Phillips, W. (1987). Thermal conductivity of ice and ice clathrate. Solid state communications, 63(2), 167-171.

Allison, M., and Clifford, S. (1987). Ice-covered water volcanism on Ganymede. J. Geophys. Res., 9(2), 7865-7876.

Amos, D., Donnelly, M., Teeratchanan, P., Bull, C., Falenty, A., et al. (2017). A chiral gas–hydrate structure common to the carbon dioxide–water and hydrogen–water systems. The Journal of Physical Chemistry Letters, 8(17), 4295-4299.

Anderson, A., Binbrek, O., and Tang, H. (1977). Raman and infrared study of the low temperature phase of solid H2S and D2S. Journal of Raman Spectroscopy, 6(5), 213-220.

Anderson, J., Lau, E., Sjogren, W., Schubert, G., Moore, W. (1996). Gravitational constraints on the internal structure of Ganymede. Nature, 384(6609), 541-543.

Andersson, O., and Inaba, A. (2005). Thermal conductivity of crystalline and amorphous ices and its implications on amorphization and glassy water. Physical Chemistry Chemical Physics, 7(7), 1441-1449.

Barr, A., and Pappalardo, R. (2005). Onset of convection in the icy Galilean satellites: Influence of rheology. Journal of Geophysical Research: Planets, 110(E12).

Barr, A., and Showman, A. (2009). Heat transfer in Europa's icy shell. In: R. T. Pallardo, W. B. McKinnon and K. Khurana (Eds.), *Europa* (pp.405-430). The University of Arizona Press, Tucson.

Berland, B., Brown, D., Tolbert, M., George, S. (1995). Refractive index and density of vapor-deposited ice. Geophysical Research Letters, 22(24), 3493-3496.

Blake, S. (1990). Viscoplastic models of lava domes. In: J. Fink (Ed.), *Lava Flows and Domes: Emplacement Mechanisms and Hazard Implications* (pp. 25-46). Springer-Verlag, New York.

Bland, M., Showman, A., Tobie, G. (2009). The orbital–thermal evolution and global expansion of Ganymede. Icarus, 200(1), 207-221.

Bridgman, P. (1912). Water, in the liquid and five solid forms, under pressure. In: *Proceedings of the American Academy of Arts and Sciences* (Vol. 47, No. 13, pp. 441-558). American Academy of Arts & Sciences.

Brown, D., George, S., Huang, C., Wong, E., Rider, K., et al. (1996). H2O condensation coefficient and refractive index for vapor-deposited ice from molecular beam and optical interference measurements. The Journal of Physical Chemistry, 100(12), 4988-4995.

Brown, R., Baines, K., Bellucci, G., Bibring, J., Buratti, B., et al. (2004). The Cassini visual and infrared mapping spectrometer (VIMS) investigation. Space Science Reviews, 115(1-4), 111-168.

Calvin, W., Clark, R., Brown, R., Spencer, J. (1995). Spectra of the icy Galilean satellites from 0.2 to 5μm: A compilation, new observations, and a recent summary. Journal of Geophysical Research: Planets, 100(E9), 19041-19048.

729 Carlson, R., Weissman, P., Smythe, W., Mahoney, J. (1992). Near-infrared mapping spectrometer
730 experiment on Galileo. Space Science Reviews, 60(1-4), 457-502.

731 Carlson, R., Anderson, M., Johnson, R., Smythe, W., Hendrix, A., et al. (1999). Hydrogen peroxide on
732 the surface of Europa. Science, 283(5410), 2062–2064.

733 Choblet, G., Tobie, G., Sotin, C., Kalousova, K., Grasset, O. (2017). Heat transport in the high-pressure
734 ice mantle of large icy moons. Icarus, 285, 252-262.

735 Choukroun, M., Kieffer, S., Lu, X., Tobie, G. (2013). Clathrate hydrates: Implications for exchange
736 processes in the outer solar system. In: M. Gudipati, J. Castillo-Rogez (Eds.), *The Science of Solar System*
737 *Ices* (pp. 409-454). Springer, New York, NY.

738 Clark, R. (1980). Ganymede, Europa, Callisto, and Saturn's rings: Compositional analysis from
739 reflectance spectroscopy. Icarus, 44(2), 388-409.

740 Clark, R., and McCord, T. (1980). The Galilean satellites: New near- infrared spectral reflectance
741 measurements (0.65 – 2.5 mm) and a 0.325 – 5 μm summary. Icarus, 41, 323–339.

742 Collins, G., Head, J., Pappalardo, R. (1998). Formation of Ganymede grooved terrain by sequential
743 extensional episodes: Implications of Galileo observations for regional stratigraphy. Icarus, 135(1), 345-
744 359.

745 Collins, G. (2000). Driving mechanisms for grooved terrain tectonics on Ganymede and chaotic terrain
746 formation on Europa: Constraints from Galileo data (Doctoral dissertation, Brown University).

747 Cook, J., and Leaist, D. (1983). An exploratory study of the thermal conductivity of methane hydrate.
748 Geophysical Research Letters, 10(5), 397-399.

749 Croft, S., and Strom, R. (1985). Ganymede's crust: Structural indicators in the Tiamat Sulcis quadrangle.
750 In: *Lunar and Planetary Science Conference* (pp. 156-157).

751 Croft, S., Lunine, J., Kargel, J. (1988). Equation of state of ammonia-water liquid: Derivation and
752 planetological applications. Icarus, 73(2), 279-293.

753 Croft, S., Kargel, J., Kirk, R., Moore, J., Schenk, P., Strom, R. (1995). The geology of Triton. In: D.
754 Cruikshank (Ed.), *Neptune and Triton*. Univ. of Ariz. Press, Tucson.

755 Dalton III, J., and Pitman, K. (2012). Low temperature optical constants of some hydrated sulfates
756 relevant to planetary surfaces. Journal of Geophysical Research: Planets, 117(E9).

757 Dartois, E., and Deboffle, D. (2008). Methane clathrate hydrate FTIR spectrum-Implications for its
758 cometary and planetary detection. Astronomy & Astrophysics, 490(3), L19-L22.

759 Dartois, E., and Schmitt, B. (2009). Carbon dioxide clathrate hydrate FTIR spectrum-Near infrared
760 combination modes for astrophysical remote detection. Astronomy & Astrophysics, 504(3), 869-873.

761 Dombard, A., and McKinnon, W. (2001). Formation of grooved terrain on Ganymede: Extensional
762 instability mediated by cold, superplastic creep. Icarus, 154(2), 321-336.

763 Dombard, A., and McKinnon, W. (2006). Elastoviscoplastic relaxation of impact crater topography with
764 application to Ganymede and Callisto. Journal of Geophysical Research: Planets, 111(E1).

765 Durham, W., and Stern, L. (2001). Rheological properties of water ice - Applications to satellites of the
766 outer planets. Annu. Rev. Earth Planet. Sci., 29, 295-330.

767 Durham, W., Stern, L., Kirby, S. (1996). Rheology of water ices V and VI. Journal of Geophysical
768 Research: Solid Earth, 101(B2), 2989-3001.

769 Durham, W., Kirby, S., Stern, L. (1997). Creep of water ices at planetary conditions: A compilation.
770 Journal of Geophysical Research: Planets, 102(E7), 16293-16302.

771 Durham, W., Kirby, S., Stern, L. (1998). Rheology of planetary ices. In: B. Schmitt, C. de Bergh, M.
772 Festou (Eds.), *Solar System Ices* (pp. 63-78). Springer, Dordrecht.

773 Durham, W., Stern, L., Kirby, S. (2001), Rheology of ice I at low stress and elevated confining pressure,
774 J. Geophys. Res.,106 (6), 11031-11042.

775 Durham, W., Stern, L., Kirby, S., Circone, S. (2005). Rheological comparisons and structural imaging of
776 sI and sII endmember gas hydrates and hydrate/sediment aggregates. In: *Proceedings of the 5th*
777 *International Conference on Gas Hydrates* (pp. 607-614). Tapir Academic.

778 Durham, W., Prieto-Ballesteros, O., Goldsby, D., Kargel, J. (2010). Rheological and thermal properties of
779 icy materials. Space science reviews, 153(1), 273-298.

780 English, N., and Tse, J. (2010). Mechanisms of thermal conduction in clathrate hydrates. In: *12th*
781 *International conference on the physics and chemistry of ice*, Abstract #6-A3-1 (Saporro).

782 Fagents, S., Greeley, R., Sullivan, R., Pappalardo, R., Prockter, L., Galileo SSI Team. (2000).
783 Cryomagmatic mechanisms for the formation of Rhadamanthys Linea, triple band margins, and other
784 low-albedo features on Europa. Icarus, 144(1), 54-88.

785 Fanale, F., Li, Y., De Carlo, E., Farley, C., Sharma, S., et al. (2001). An experimental estimate of
786 Europa's "ocean" composition independent of Galileo orbital remote sensing. Journal of Geophysical
787 Research: Planets, 106(E7), 14595-14600.

788 Fortes, A., and Choukroun, M. (2010). Phase behaviour of ices and hydrates. Space science reviews,
789 153(1-4), 185-218.

790 Fortes, A., Wood, I., Sclater, G., Tucker, M. (2010). Recovery and characterization of high-pressure
791 phases in the systems H2O–NH3, H2O–H2SO4, and H2O–MgSO4. ISIS Experimental Report,
792 Rutherford Appleton Laboratory, 1010009.

793 Fray, N., and Schmitt, B. (2009). Sublimation of ices of astrophysical interest: A bibliographic review.
794 Planetary and Space Science, 57(14-15), 2053-2080.

795 Giauque, W., and Stephenson, C. (1938). Sulfur dioxide. The heat capacity of solid and liquid. Vapor
796 pressure. Heat of vaporization. The entropy values from thermal and molecular data. Journal of the
797 American Chemical Society, 60(6), 1389-1394.

798 Giovambattista, N., Amann-Winkel, K., Loerting, T. (2013). Amorphous ices. Liquid Polymorphism,
799 152, 139-173.

800 Goldsby, D., and Kohlstedt, D. (2001). Superplastic deformation of ice: Experimental observations. J.
801 Geophys. Res. Solid Earth, 106(B6), 11017-11030.

802 Golombek, M. (1982). Constraints on the expansion of Ganymede and the thickness of the lithosphere.
803 Journal of Geophysical Research: Solid Earth, 87(S01), A77-A83.

804 Grimm, R., and Squyres, S. (1985). Spectral analysis of groove spacing on Ganymede. Journal of
805 Geophysical Research: Solid Earth, 90(B2), 2013-2021.

806 Grundy, W., and Schmitt, B. (1998). The temperature-dependent near-infrared absorption spectrum of
807 hexagonal H2O ice. Journal of Geophysical Research: Planets, 103(E11), 25809-25822.

808 Grundy, W., Buie, M., Stansberry, J., Spencer, J., Schmitt, B. (1999). Near-infrared spectra of icy outer
809 solar system surfaces: Remote determination of H2O ice temperatures. Icarus, 142(2), 536-549.

810 Grundy, W., Buratti, B., Cheng, A., Emery, J., Lunsford, A., et al. (2007). New Horizons mapping of
811 Europa and Ganymede. Science, 318, 234.

812 Han, L., and Showman, A. (2008). Implications of shear heating and fracture zones for ridge formation on
813 Europa. Geophysical Research Letters, 35(3).

814 Hansen, G., and McCord, T. (2004). Amorphous and crystalline ice on the Galilean satellites: A balance
815 between thermal and radiolytic processes. Journal of Geophysical Research, 109, E01012.

816 Hanson, D., and Mauersberger, K. (1986). The vapor pressures of solid and liquid ozone. The Journal of
817 chemical physics, 85(8), 4669-4672.

818 Hapke, B. (1993). *Theory of reflectance and emittance spectroscopy*. Cambridge, UK: Cambridge
819 University Press.

820 Hartmann, W. (1980). Surface evolution of two-component stone/ice bodies in the Jupiter region. Icarus,
821 44(2), 441-453.

822 Hendrix, A., Barth, C., Stewart, A., Hard, C., Lane, A. (1999). Hydrogen peroxide on the icy Galilean
823 satellites. In: *Lunar and Planetary Science Conference*, Abstracts p. 2043.

824 Hendrix, A., Domingue, D., Noll, K. (2013). Ultraviolet properties of planetary ices. In: M. Gudipati, J.
825 Castillo-Rogez (Eds.), *The Science of Solar System Ices* (pp. 73-105). Springer, New York, NY.

826 Hibbitts, C., Pappalardo, R., Hansen, G., McCord, T. (2003). Carbon dioxide on Ganymede. Journal of
827 Geophysical Research, 108(5), 5036.

828 Hirai, H., Komatsu, K., Honda, M., Kawamura, T., Yamamoto, Y., Yagi, T. (2010). Phase changes of CO
829 2 hydrate under high pressure and low temperature. The Journal of chemical physics, 133(12), 124511.

830 Hogenboom, D., Kargel, J., Ganasan, J., Lee, L. (1995). Magnesium sulfate-water to 400 MPa using a
831 novel piezometer: Densities, phase equilibria, and planetological implications. Icarus, 115(2), 258-277.

832 Hudleston, P. (2015). Structures and fabrics in glacial ice: A review. Journal of Structural Geology, 81, 1-
833 27.

834 Huebner, W., Benkhoff, J., Capria, M., Coradini, A., De Sanctis, C., et al. (2006). Heat and gas diffusion
835 in comet nuclei (Vol. 133). Bern: International Space Science Institute.

836 Huppert, H., Shepherd, J., Sigurdsson, R., Sparks, S. (1982). On lava dome growth, with application to
837 the 1979 lava extrusion of the Soufriere of St. Vincent. Journal of Volcanology and Geothermal Research,
838 14(3-4), 199-222.

839 Hussmann, H., Sohl, F., Spohn, T. (2006). Subsurface oceans and deep interiors of medium-sized outer
840 planet satellites and large trans-neptunian objects. Icarus, 185(1), 258-273.

841 Jankowski, D., and Squyres, S. (1988). Solid-state ice volcanism on the satellites of Uranus. Science,
842 241(4871), 1322-1325.

843 Jenniskens, P., and Blake, D. (1994). Structural transitions in amorphous water ice and astrophysical
844 implications. Science, 265(5173), 753-756.

845 Jenniskens, P., Blake, D., Kouchi, A. (1998). Amorphous water ice. In: B. Schmitt, C. de Bergh, M.
846 Festou (Eds.), *Solar System Ices* (pp. 139-155). Springer, Dordrecht.

847 Johnson, R., and Jesser, W. (1997). O2/O3 microatmospheres in the surface of Ganymede. The
848 Astrophysical Journal Letters, 480(1), L79.

849 Journaux, B., Daniel, I., Caracas, R., Montagnac, G., Cardon, H. (2013). Influence of NaCl on ice VI and
850 ice VII melting curves up to 6 GPa, implications for large icy moons. Icarus, 226(1), 355-363.

851 Journaux, B., Daniel, I., Petitgirard, S., Cardon, H., Perrillat, J., et al. (2017). Salt partitioning between
852 water and high-pressure ices. Implication for the dynamics and habitability of icy moons and water-rich
853 planetary bodies. Earth and Planetary Science Letters, 463, 36-47.

854 Journaux, B., Kalousová, K., Sotin, C., Tobie, G., Vance, S., et al. (2020). Large ocean worlds with high-
855 pressure ices. Space Science Reviews, 216(1), 1-36.

856 Kalousová, K., and Sotin, C. (2018). Melting in High-Pressure Ice Layers of Large Ocean Worlds—
857 Implications for Volatiles Transport. Geophysical Research Letters, 45(16), 8096-8103.

858 Kalousová, K., Sotin, C., Choblet, G., Tobie, G., Grasset, O. (2018). Two-phase convection in
859 Ganymede's high-pressure ice layer—Implications for its geological evolution. Icarus, 299, 133-147.

860 Kamata, S., Nimmo, F., Sekine, Y., Kuramoto, K., Noguchi, N., et al. (2019). Pluto's ocean is capped and
861 insulated by gas hydrates. Nature Geoscience, 12(6), 407-410.

862 Kargel, J. (1998). Physical chemistry of ices in the outer solar system. In: B. Schmitt, C. de Bergh, M.
863 Festou (Eds.), *Solar system ices* (pp. 3-32). Springer, Dordrecht.

864 Kargel, J., Croft, S., Lunine, J., Lewis, J. (1991). Rheological properties of ammonia-water liquids and
865 crystal-liquid slurries: Planetological applications. Icarus, 89(1), 93-112.

866 Kargel, J., Kaye, J., Head III, J., Marion, G., Sassen, R., et al. (2000). Europa's crust and ocean: origin,
867 composition, and the prospects for life. Icarus, 148(1), 226-265.

868 Kieffer, H., and Smythe, W. (1974). Frost spectra: Comparison with Jupiter's satellites. Icarus, 21, 506–
869 512.

870 Kivelson, M., Khurana, K., Volwerk, M. (2002). The permanent and inductive magnetic moments of
871 Ganymede. Icarus, 157(2), 507-522.

872 Klinger, J., Whalley, E., Jones, S., Gold, L. (1973). Thermal conductivity of ice single crystals at low
873 temperatures. Physics and Chemistry of Ice. Royal Society of Canada, Ottawa, 114-116.

874 Kouchi, A., Greenberg, J., Yamamoto, T., Mukai, T. (1992). Extremely low thermal conductivity of
875 amorphous ice-Relevance to comet evolution. The Astrophysical Journal, 388, L73-L76.

876 Kubo, T., Nakata, H., Kato, T. (2009). Effects of insoluble particles on grain growth in polycrystalline
877 ice: Implications for rheology of ice shells of icy satellites. Journal of Mineralogical and Petrological
878 Sciences, 104(5), 301-306.

879 Leonteva, A., Stroilov, Y., Lakin, E., Bolshutkin, D. (1970). Zero point oscillation energy effect on
880 plastic deformation in solidified gases. Physica status solidi (b), 42(2), 543-549.

881 Ligier, N., Paranicas, C., Carter, J., Poulet, F., Calvin, W. M., et al. (2019). Surface composition and
882 properties of Ganymede: Updates from ground-based observations with the near-infrared imaging
883 spectrometer SINFONI/VLT/ESO. Icarus, 333, 496–515.

884 Lorenz, R., and Shandera, S. (2001). Physical properties of ammonia-rich ice: Application to Titan.
885 Geophysical research letters, 28(2), 215-218.

886 Lucchita, B. (1980). Grooved terrain on Ganymede. Icarus, 44(2), 481-501.

887 Lucchitta, B., Barnes, C., Glotfelty, M. (1992). Geological map of the Memphis Facula quadrangle (Jg-7)
888 of Ganymede, U. S. Geol. Surv. Map. 1-2289, Jg-9.

889 Luna, R., Satorre, M., Santonja, C., Domingo, M. (2014). New experimental sublimation energy
890 measurements for some relevant astrophysical ices. Astronomy & Astrophysics, 566, A27.

891 Lunine, J., and Stevenson, D. (1982). Formation of the Galilean satellites in a gaseous nebula. Icarus,
892 52(1), 14-39.

893 Macmillan, N. (1972). The theoretical strength of solids. Journal of Materials Science, 7(2), 239-254.

894 Massani, B., Mitterdorfer, C., Loerting, T. (2017). Formation and decomposition of CO2-filled ice. The
895 Journal of chemical physics, 147(13), 134503.

896 Mastrapa, R., Grundy, W., Gudipati, M. (2013). Amorphous and Crystalline H 2 O-Ice. In: M. Gudipati,
897 J. Castillo-Rogez (Eds.), *The science of solar system ices* (pp. 371-408). Springer, New York, NY.

898 McCord, T., Hansen, G., Clark, R., Martin, P., Hibbitts, C., et al. (1998). Non-water ice constituents in
899 the surface material of the icy Galilean satellites from the Galileo near-infrared mapping spectrometer
900 investigation. Journal of Geophysical Research, 103(E4), 8603–8626.

901 McCord, T., Hansen, G., Hibbitts, C. (2001). Hydrated salt minerals on Ganymede's surface: Evidence of
902 an ocean below. Science, 292(5521), 1523–1525. https://doi.org/10.1126/science.1059916

903 McKinnon, W. (1999). Convective instability in Europa's floating ice shell. Geophysical Research
904 Letters, 26(7), 951-954.

905 McKinnon, W., and Melosh, H. (1980). Evolution of planetary lithospheres: Evidence from multiringed
906 structures on Ganymede and Callisto. Icarus, 44(2), 454-471.

907 Melosh, H., and Janes, D. (1989). Ice volcanism on Ariel. Science, 245(4914), 195-196.

908 Mullins, J., Ziegler, W., Kirk, B. (1963). The thermodynamic properties of oxygen from 20 to 100 K. In:
909 K. Timmerhaus (Ed.), *Advances in Cryogenic Engineering* (pp. 126-134). Springer, Boston, MA.

910 Mura, A., Adriani, A., Sordini, R., Sindoni, G., Plainaki, C., et al. (2020). Infrared Observations of
911 Ganymede From the Jovian InfraRed Auroral Mapper on Juno. Journal of Geophysical Research: Planets,
912 125(12), e2020JE006508.

913 Murchie, S., Head, J., Helfenstein, P., Plescia, J. (1986). Terrain types and local-scale stratigraphy of
914 grooved terrain on Ganymede. Journal of Geophysical Research: Solid Earth, 91(B13), E222-E238.

915 Murchie, S., Head, J., Plescia, J. (1989). Crater densities and crater ages of different terrain types on
916 Ganymede. Icarus, 81(2), 271-297.

917 Murchie, S., Head, J., Plescia, J. (1990). Tectonic and volcanic evolution of dark terrain and its
918 implications for the internal structure and evolution of Ganymede. Journal of Geophysical Research:
919 Solid Earth, 95(B7), 10743-10768.

920 Murphy, D., and Koop, T. (2005). Review of the vapour pressures of ice and supercooled water for
921 atmospheric applications. Quarterly Journal of the Royal Meteorological Society: A journal of the
922 atmospheric sciences, applied meteorology and physical oceanography, 131(608), 1539-1565.

923 Nakamura, R., and Ohtani, E. (2011). The high-pressure phase relation of the MgSO4–H2O system and
924 its implication for the internal structure of Ganymede. Icarus, 211(1), 648-654.

925 Nakano, S., Moritoki, M., Ohgaki, K. (1998). High-pressure phase equilibrium and Raman microprobe
926 spectroscopic studies on the CO2 hydrate system. Journal of chemical & engineering data, 43(5), 807-
927 810.

928 Narten, A., Venkatesh, C., Rice, S. (1976). Diffraction pattern and structure of amorphous solid water at
929 10 and 77 K. The Journal of Chemical Physics, 64(3), 1106-1121.

930 Nelson, R., Lane, A., Matson, D., Veeder, G., Buratti, B., Tedesco, E. (1987). Spectral geometric albedos
931 of the Galilean satellites from 0.24 to 0.34 micrometers: Observations with the International Ultraviolet
932 Explorer. Icarus, 72(2), 358-380.

933 Nimmo, F., Pappalardo, R., Giese, B. (2002). Effective elastic thickness and heat flux estimates on
934 Ganymede. Geophysical Research Letters, 29(7), 62-1.

935 Noll, K., Johnson, R., Lane, A., Domingue, D., Weaver, H. (1996). Detection of ozone on Ganymede.
936 Science, 273(5273), 341-343.

937 Palumbo, M. (2005). The morphology of interstellar water ice. In: *Journal of Physics: Conference Series*,
938 6 (1), p. 025.

939 Pappalardo, R., Head, J., Collins, G., Kirk, R., Neukum, G., et al. (1998). Grooved terrain on Ganymede:
940 First results from Galileo high-resolution imaging. Icarus, 135(1), 276-302.

941 Pappalardo, R., Nimmo, F., Giese, B., Bader, C., Deremer, L., Prockter, L. (2003). Furrow Topography
942 and the Elastic Thickness of Ganymede's Dark Terrain Lithosphere. In: *Lunar and Planetary Science*
943 *Conference* (p. 1511).

944 Pappalardo, R., Collins, G., Head, J., Helfenstein, P., McCord, T., et al. (2004). Geology of Ganymede.
945 In: F. Bagenal, T. Dowling, W. McKinnon (Eds.), *Jupiter* (pp. 363–396). Cambridge, UK: Cambridge
946 University Press.

947 Parmentier, E., Squyres, S., Head, J., Allison, M. (1982). The tectonics of Ganymede. Nature, 295(5847),
948 290-293.

949 Patel, J., Pappalardo, R., Head, J., Collins, G., Hiesinger, H., Sun, J. (1999). Topographic wavelengths of
950 Ganymede groove lanes from Fourier analysis of Galileo images. Journal of Geophysical Research:
951 Planets, 104(E10), 24057-24074.

952 Patterson, G., Collins, G., Head, J., Pappalardo, R., Prockter, L., et al. (2010). Global geological mapping
953 of Ganymede. Icarus, 207(2), 845-867.

954 Petrenko, V., and Whitworth, R. (1999). *Physics of ice*. OUP Oxford.

955 Poirier, J. (1985). *Creep of crystals: high-temperature deformation processes in metals, ceramics and*
956 *minerals.* Cambridge University Press.

957 Pollack, J., Witteborn, F., Erickson, E., Strecker, D., Baldwin, B., Bunch, T. (1978). Near-infrared spectra
958 of the Galilean satellites: Observations and compositional implications. Icarus, 36, 271–303.

959 Prockter, L., and Pappalardo, R. (2000). Folds on Europa: Implications for crustal cycling and
960 accommodation of extension. Science, 289(5481), 941-943.

961 Prockter, L., Figueredo, P., Pappalardo, R., Head, J., Collins, G. (2000). Geology and mapping of dark
962 terrain on Ganymede and implications for grooved terrain formation. Journal of Geophysical Research:
963 Planets, 105(E9), 22519-22540.

964 Ross, R., and Kargel, J. (1998). Thermal conductivity of solar system ices, with special reference to
965 Martian polar caps. In: B. Schmitt, C. de Bergh, M. Festou (Eds.), *Solar system ices* (pp. 33-62). Springer,
966 Dordrecht.

967 Ross, R., Andersson, P., Bäckström, G. (1981). Unusual PT dependence of thermal conductivity for a
968 clathrate hydrate. Nature, 290(5804), 322-323.

969 Safarik, D., and Mullins, C. (2004). The nucleation rate of crystalline ice in amorphous solid water. The
970 Journal of chemical physics, 121(12), 6003-6010.

971 Schenk, P., and McKinnon, W. (1991). Dark-ray and dark-floor craters on Ganymede, and the provenance
972 of large impactors in the Jovian system. Icarus, 89(2), 318-346.

973 Schenk, P., and Moore, J. (1995). Volcanic constructs on Ganymede and Enceladus: Topographic
974 evidence from stereo images and photoclinometry. Journal Geophysical Research, 100 (E9), 19009 –
975 19022.

976 Schenk, P., McKinnon, W., Gwynn, D., Moore, J. (2001). Flooding of Ganymede's bright terrains by low-
977 viscosity water-ice lavas. Nature, 410(6824), 57-60.

978 Schenk, P., Chapman, C., Zahnle, K., Moore, J. (2004). Ages and interiors: The cratering record of the
979 Galilean satellites. Jupiter: The planet, satellites and magnetosphere, 2, 427.

980 Schmitt, B., Quirico, E., Trotta, F., Grundy, W. (1998). Optical properties of ices from UV to infrared. In:
981 B. Schmitt, C. de Bergh, M. Festou (Eds.), *Solar System Ices* (pp. 199-240). Springer, Dordrecht.

982 Schulson, E. (1979). An analysis of the brittle to ductile transition in polycrystalline ice under tension.
983 Cold Regions Science and Technology, 1(2), 87-91.

984 Shoemaker, E., Lucchita, B., Wilhelms, D., Plescia, J., Squyres, S. (1982). The geology of Ganymede. In:
985 D. Morrison (Ed.), *Satellites of Jupiter* (pp. 435-520). Univ. of Ariz. Press, Tucson.

Sloan, E., and Koh, C. (2007) *Clathrate hydrates of natural gases*. 3rd ed. CRC press, Boca Raton.

Smith, B., Soderblom, L., Batson, R., Bridges, P., Inge, J., et al. (1982). A new look at the Saturn system: The Voyager 2 images. Science, 215(4532), 504-537.

Smith, B., Soderblom, L., Beebe, R., Bliss, D., Boyce, J., et al. (1986). Voyager 2 in the Uranian system: Imaging science results. Science, 233(4759), 43-64.

Sohl, F., Choukroun, M., Kargel, J., Kimura, J., Pappalardo, R., et al. (2010). Subsurface water oceans on icy satellites: Chemical composition and exchange processes. Space Science Reviews, 153(1), 485-510.

Solomatov, V. (1995). Scaling of temperature-and stress-dependent viscosity convection. Physics of Fluids, 7(2), 266-274.

Sotin, C., and Poirier, J. (1987). Viscosity of ice V. Le Journal de Physique Colloques 48(C1), 233-238.

Sotin, C., Gillet, P., Poirier, J. (1985). Creep of High-Pressure Ice VI. In: J. Klinger, D. Benest, A. Dollfus, R. Smoluchowski (Eds.), *Ices in the Solar System* (pp. 109-118), Springer Netherlands, Dordrecht.

Spencer, J. (1987). Icy Galilean satellite reflectance spectra: Less ice on Ganymede and Callisto?. Icarus, 70(1), 99-110.

Spencer, J., Calvin, W., Person, M. (1995). CCD spectra of the Galilean satellites: Molecular oxygen on Ganymede (Paper 95JE01503). Journal of Geophysical Research-Part E-Planets-Printed Edition, 100(9), 19049-19056.

Squyres, S. (1980). Topographic domes on Ganymede: Ice vulcanism or isostatic upwarping. Icarus, 44(2), 472-480.

Squyres, S., Reynolds, R., Cassen, P., Peale, S. (1983). Liquid water and active resurfacing on Europa. Nature, 301(5897), 225-226.

Stephan, K., Ciarniello, M., Poch, O., Schmitt, B., Haack, D., Raponi, A. (2021). Spectral Properties of H2O Ice Depending on Particle Sizes and Temperatures Expected on Ganymede and Callisto. In: *Lunar and Planetary Science Conference* (No. 2548, p. 1341).

Stern, L., Kirby, S., Durham, W. (1996). Peculiarities of methane clathrate hydrate formation and solid-state deformation, including possible superheating of water ice. Science, 273(5283), 1843-1848.

Stevenson, D., and Lunine, J. (1986). Mobilization of cryogenic ice in outer solar system satellites. Nature, 323(6083), 46-48.

Strazzulla, G. (2011). Cosmic ion bombardment of the icy moons of Jupiter. Nuclear Instruments and Methods in Physics Research Section B: Beam Interactions with Materials and Atoms, 269(9), 842-851.

Strazzulla, G., Garozzo, M., Gomis, O. (2009). The origin of sulfur-bearing species on the surfaces of icy satellites. Advances in space research, 43(9), 1442-1445.

Sugisaki, M., Suga, H., Seki, S. (1969). Calorimetric study of glass transition of the amorphous ice and of the phase transformation between the cubic and hexagonal ices. Physics of Ice. Platinum Press, New York, 329-343.

1022 Sumarokov, V., Stachowiak, P., Jeżowski, A. (2003). Low-temperature thermal conductivity of solid
1023 carbon dioxide. Low Temperature Physics, 29(5), 449-450.

1024 Thomas, P., and Schubert, G. (1988). Power law rheology of ice and the relaxation style and retention of
1025 craters on Ganymede. Journal of Geophysical Research: Solid Earth, 93(B11), 13755-13762.

1026 Tse, J., White, M. (1988). Origin of glassy crystalline behavior in the thermal properties of clathrate
1027 hydrates: a thermal conductivity study of tetrahydrofuran hydrate. The Journal of Physical Chemistry,
1028 92(17), 5006-5011.

1029 Umurhan, O., Ahrens, C., Chevrier, V. (2021). Rheological and thermophysical properties and some
1030 processes involving common volatile materials found on Pluto's surface. In: S. Stern, R. Binzel, W.
1031 Grundy, J. Moore, L. Young (Eds.), *The Pluto System After New Horizons*. University of Arizona Press.

1032 Vance, S., and Brown, J. (2013). Thermodynamic properties of aqueous MgSO4 to 800 MPa at
1033 temperatures from− 20 to 100 C and concentrations to 2.5 mol kg− 1 from sound speeds, with
1034 applications to icy world oceans. Geochimica et Cosmochimica Acta, 110, 176-189.

1035 Vance, S., Bouffard, M., Choukroun, M., Sotin, C. (2014). Ganymede's internal structure including
1036 thermodynamics of magnesium sulfate oceans in contact with ice, Planet. Space Sci., 96, 62-70.

1037 Vance, S., Panning, M., Sthler, S., Cammarano, F., Bills, B., et al. (2018). Geophysical investigations of
1038 habitability in ice-covered ocean worlds. J. of Geophys. Res. Planets, 123(1), 180-205.

1039 Wagner, W., and Pruss, A. (2002). The IAPWS formulation 1995 for the thermodynamic properties of
1040 ordinary water substance for general and scientific use. Journal of physical and chemical reference data,
1041 31(2), 387-535.

1042 Washburn, E. (1924). The vapor pressure of ice and of water below the freezing point. Monthly Weather
1043 Review, 52(10), 488-490.

1044 Yamamoto, T., Nakagawa, N., Fukui, Y. (1983). The chemical composition and thermal history of the ice
1045 of a cometary nucleus. Astronomy and Astrophysics, 122, 171-176.

1046 Yamashita, Y., Kato, M., Arakawa, M. (2010). Experimental study on the rheological properties of
1047 polycrystalline solid nitrogen and methane: Implications for tectonic processes on Triton. Icarus, 207(2),
1048 972-977.

1049 Zahnle, K., Schenk, P., Levison, H., Dones, L. (2003). Cratering rates in the outer Solar System. Icarus,
1050 163(2), 263-289.

1051 Zolotov, M., and Shock, E. (2001). Composition and stability of salts on the surface of Europa and their
1052 oceanic origin. Journal of Geophysical Research: Planets, 106(E12), 32815-32827.